Neurophysiological activity patterns associated with excessive motor behaviors during long-term dopaminergic pharmacotherapy in a primate model of Parkinson's disease

Mariana Araujo
IINELS - Instituto Internacional de Neurociências Edmond e Lily Safra
Gulraiz Iqbal Choudhary
Umeå University
Love Zackrisson
Umeå University
Luciano Censoni
Umeå University
José Firmino Rodrigues Neto
IINELS - Instituto Internacional de Neurociências Edmond e Lily Safra
Manuela Sales Lima Nascimento
IINELS - Instituto Internacional de Neurociências Edmond e Lily Safra
Pär Halje
Lund University
Romulo Fuentes Flores
Universidad de Chile
Per Petersson
per.petersson@umu.se

Umeå University

Article

Keywords: Levodopa, Oxidopamine, Electrophysiology, Dyskinesia Drug-Induced

Posted Date: May 6th, 2026

DOI: https://doi.org/10.21203/rs.3.rs-8895219/v1

Additional Declarations: No competing interests reported.

Abstract

Dopamine replacement therapy remains the main treatment for Parkinson's disease (PD), but long-term use is associated with motor fluctuations and dyskinesia severely limiting therapeutic efficacy. In addition, late-stage PD patients often suffer from non-motor symptoms exacerbated by dopamine replacement therapy, such as PD-related psychosis (PD-P). In recent years, neurophysiological activity patterns associated with dyskinesia and psychosis have been identified in rodent models of PD, opening up opportunities for more mechanistic studies of these troublesome side effects. To determine whether long-term levodopa treatment in parkinsonian primates is associated with maladaptive circuit changes promoting pathophysiological brain activity similar to the rodent models, two unilaterally 6-OHDA-lesioned marmosets (Callithrix jacchus) were chronically implanted with recording electrodes in different parts of the cortico-basal ganglia-thalamic circuits, and behavior and neurophysiological activity were monitored in association with dopaminergic pharmacotherapy over one year. Levodopa alleviated signs of PD, but also induced excessive motor behaviors, including signs of PD-P. Concomitantly, beta-band local field potential activity was reduced and in one animal distinct narrow-band gamma oscillations developed in the subthalamic nucleus. Changes in subthalamic single-unit activity associated with levodopa treatment were dominated by increased firing rates that became more pronounced after a few months of treatment. Based on these observations, we propose that oscillatory activity in the high gamma-band and increased firing rates in a subgroup of subthalamic neurons should be further investigated as potential pathophysiological factors underlying drug-induced hyperkinetic and psychotic symptoms in PD.

Introduction

Levodopa (L-DOPA) remains the main symptomatic treatment of Parkinson's disease (PD). However, after an initial stable motor response to L-DOPA, long-term therapy is often associated with motor fluctuations and the display of excessive motor activity, including dyskinesia and dystonia (Fabbrini *et al.*, 2007). In accordance with clinical observations, excessive motor activity is also commonly observed after prolonged L-DOPA treatment in animal models of PD (Visanji et al., 2009; Winkler et al., 2002). It remains to be determined which changes at the cellular and circuit level are primarily underlying the altered response to dopaminergic stimulation, but a few key mechanisms have been proposed. These encompass, for example, dysregulation of dopamine release following conversion of L-DOPA to dopamine by serotonergic cells (Carta et al., 2007; Sellnow et al., 2019), a supersensitivity to dopamine in striatum (Cenci, 2007) and other motor structures (Halje et al., 2012), and enhanced activity in striatal projection neurons, particularly in the direct pathway (Alcacer et al., 2016, 2025; Ryan et al., 2018). In addition, changes in glutamatergic signaling in the corticostriatal system have been implicated (Calon et al., 2003; Ryan et al., 2024).

Neurophysiological recordings from cortico-basal ganglia circuits in PD patients and in animal models of PD have shown that L-DOPA treatment acutely decreases beta (13–35 Hz) oscillatory activity and concurrently induces a relative increase in the power of oscillations both in the theta band (6-9Hz;

Alonso-Frech et al., 2006; Petersson et al., 2020; Tamtè et al., 2016) and in a narrow part of the gamma band (70–90 Hz; Brown et al., 2001). These latter oscillations appear to be particularly pronounced in subjects with levodopa-induced dyskinesia (Halje et al., 2012; Petersson et al., 2019; Swann et al., 2016). Moreover, in rodent models of PD, a gradual increase in the power of narrowband gamma oscillations (NBGs) over time has been demonstrated in a chronic L-DOPA treatment regimen (Dupre et al., 2015; Güttler et al., 2021), indicating maladaptive network changes associated with prolonged dopamine treatment may be contributing to the development of both NBGs and motor complications. Once a pathophysiological response to L-DOPA is established, excessive motor activity such as chorea or dystonia can be induced also by direct activation of either D1-type or D2-type dopamine receptors, independently, using more selective dopamine receptor agonists (Skovgård et al., 2023). Importantly, chronic dopaminergic stimulation affects not only motor circuits but also cognitive-limbic networks (Weintraub, 2020), suggesting that similar maladaptive changes may contribute to non-motor complications.

In PD, psychiatric complications are very common in advanced stages and constitute a major problem for many patients and their caregivers (Fénelon & Alves, 2010; Zahodne & Fernandez, 2010). Moreover, some of these complications are exacerbated by dopamine replacement therapy (Fénelon & Alves, 2010; Forsaa et al., 2010). The need for a better understanding of these ‘non-motor’ symptoms in PD is therefore increasingly being recognized as a prioritized research question (Batzu et al., 2024). However, for obvious reasons, neuropsychiatric conditions can be particularly difficult to study in animal models. Yet, behavioral and ethological studies in non-human primates revealing very human-like behavioral manifestations of neuropsychiatric conditions have opened up opportunities for more advanced translational investigations (Dettmer & Suomi, 2014; Nelson & Winslow, 2008). In particular, in the marmoset non-human primate model of PD, validated rating scales have been developed for the purpose of quantifying the expression of behaviors thought to reflect symptoms in the cognitive-limbic domain (Fox et al., 2010; Visanji et al., 2009).

Expanding on these findings, we have here characterized how brain activity patterns change both acutely with L-DOPA treatment and as a consequence of long-term dopaminergic pharmacotherapy in the 6-OHDA marmoset model of PD, in association with different abnormal behaviors, including signs of both dyskinesia and of PD-related psychosis (PD-P). Our results suggest STN firing rate changes and gamma-band oscillations may be contributing to these symptoms.

Materials and methods

Animals

Two adult female common marmosets (*Callithrix jacchus*) 300-550g were used in the study. The animals were housed in pairs in cages (1.0 x 1.0 x 2.3 m) in a vivarium with natural light cycle (12/12 hours) and outdoor temperature. All animal procedures were carried out according to approved protocols by ISD

Ethics Committee No. 02/2015AAS and strictly in accordance with the National Institute of Health Guide for the Care and Use of Laboratory Animals (NIH Publications No. 80 – 23).

Surgical procedures

All surgical procedures were carried out under antiseptic conditions. Animals were initially sedated with ketamine (10–20 mg/kg i.m.) and Atropine (0.05 mg/kg i.m.) followed by deep anesthesia with isoflurane 1–5% in oxygen at 1-1.5 L/min during the surgery.

6-OHDA lesions - Two microliters of 6-OHDA solution (4 mg/mL, 0.05% ascorbic acid, saline) was injected with a 32 gauge syringe at 0.5 µL/min into the left medial forebrain bundle in the following five locations (interaural AP/ML/DV): 6.5/1.2/6.0; 6.5/1.2/7.0; 6.5/2.2/6.5; 6.5/2.2/7.5; 6.5/3.2/8.0 (Annett et al., 1992). Anteroposterior coordinates were corrected according to the dimensions of the skull of each animal (Stephan et al., 1980). Following surgery, the animals received non-steroid anti-inflammatory analgesic (flunixin meglumine 1mg/kg, s.c.) for 3 days, dexamethasone (0.5–1mg/kg, i.m.) for 5 days and enrofloxacin (5 mg/kg, s.c.) for 7 days.

Implantation of recording electrodes - Six small holes were drilled in the cranium for insertion of stainless steel screws used to secure the implant and serve as ground connections for later recordings. Two craniotomies for the electrode arrays in each hemisphere were then performed. Meninges were carefully removed, and the cortical surface was kept wet using sterile gauze soaked with saline solution. Micro-wire electrodes were stereotactically implanted using a micromanipulator (Santana et al., 2014). The structures targeted, as verified by histological verification (Stephan et al., 1980) were: primary somatosensory and motor and the premotor cortical areas, putamen, globus pallidus pars interna/externa, zona incerta and the subthalamic nucleus, and thalamic nuclei including: the ventral posterolateral, ventrolateral, pulvinar and the medial geniculate nucleus (see **Supplementary Table 1**). After implantation, electrodes and connectors were fixed to the skull with dental acrylic.

Pharmacological treatments

Animals were injected with 20–200 mg/kg L-DOPA with 37.5 mg/kg Benserazide, s.c. in saline solution during light isoflurane anesthesia. Additionally, one of the animals (Monkey 2) was temporarily switched to apomorphine treatment (0.3–2.0 mg/kg) during a 3-week period to evaluate potential differences between L-DOPA and dopamine agonist treatment.

Behavioral assessments - automatized quantification of locomotive behavior

Spontaneous motility and locomotor bouts in the horizontal plane during neurophysiological recording sessions were quantified using automated procedures with custom-developed software in Python and

MATLAB. Following previously described methods (Palmér et al., 2017), the animal's outer boundaries were segmented in the x-y plane for each video frame (80 frames per second), and the coordinates of a fitted centroid were calculated. To construct a coarse measure of motility, data were smoothed and subsampled to 1 Hz (1/80), and the absolute value of coordinate differentials—representing differences in centroid positions 1 second apart—served as the metric for motility or speed. Locomotor bouts were then extracted using a threshold of 6 cm/second derived from the histogram of all motility values for each monkey. The distance travelled and frequency per session of these bouts were quantified and compared between baseline and L-DOPA conditions. The same comparison was performed on the full distribution of speed values (without thresholding). These analyses were conducted for the first 16 minutes of baseline recording and the 16-to-32-minute interval following L-DOPA injection.

Behavioral assessments - manual quantification of behavioral features

In addition to the automatized measures from motion tracking of video recordings, a number of more specific behaviors, indicative of parkinsonism, dyskinesia, hyperkinesia or PD-P were scored manually (assessed for one minute, every fifth minute) according to the severity scales described below.

Parkinsonism: To assess alleviation of parkinsonism, we primarily relied on automated tracking of spontaneous behavior. However, Monkey B also displayed clear signs of cervical dystonia in the untreated state. Specifically, the neck was laterally flexed to the right but rotated to the left so that the animal was facing upwards to the left (torticollis). This symptom did not display any spasmodic episodes and was completely reversed by dopaminergic treatment **(Supplementary Video 1)**. Hence, this postural sign was used as an indicator of parkinsonism in this animal. Symptom severity for torticollis was graded according to the time head tilt/torticollis was present during each 1-min observation window according to the following ordinal scale: [0 – absent; 1–1-20s/min; 2 = 21-40s/min; 3 = 41-60s/min].

L-DOPA- and apomorphine-induced behaviors

Dyskinetic signs: In this model of PD, we found that dystonia appears to be the dominating sign of dyskinesia rather than chorea. Abnormal dystonic posture of the neck and head was observed in both animals after pharmacological treatment. However, in contrast to the untreated state, the head was rotated to the right (contralateral to the lesion). More severe dyskinesia also included spasmodic episodes (characterized by periodic jerking, turning movements to the right). These spasmodic episodes sometimes also involved the forelimbs, although this was more rarely observed **(Supplementary Video 2, 3)**. Symptom severity of these dyskinetic/dystonic signs were graded according to both intensity and duration during each 1-min observation window, according to the following ordinal scales:

Intensity

[0 – Absent; 1 - Cervical dystonia where the head is rotated to the right during prolonged periods; 2 - Pronounced head turning to the right (face is directed partly backwards). Small neck spasms occur sporadically; 3 - Head rotated to the right with periodic jerking motions of the neck in the same direction, or head rotated so far to the right that the animal needs to adjust its forelimbs not to fall over. Spasms occur sporadically also in the forelimbs.]

Duration

[0 – absent; 1–1-20s/min; 2 = 21-40s/min; 3 = 41-60s/min].

Rotations: In conjunction with the above described dyskinetic signs, animals often displayed whole-body rotations contraversive to the lesion, indicative of drug-induced hyperkinesia **(Supplementary Video 4, 5)**. The number of body rotations were counted during each 1-min observation window. To facilitate manual scoring, a half full rotation was used as the counted units (defined as 180° body rotation towards the side contralateral to the lesion). These numbers were later converted into an ordinal scale (1–7 = 1; 8–15 = 2; 16–23 = 3).

Locomotion: was here broadly defined as including any type of movement resulting in net translation of the whole body. Examples of this would be rearing, walking, climbing, jumping, rotations, but also behaviors that might rather be considered as signs of non-motor symptoms (agitated rapid locomotion and escape-like behavior). In contrast, more restricted movements involving the head and neck were consequently not included in this category. Locomotion was scored by the observer on an ordinal scale from 0–4; Duration: [0 s/min – Absent; 1–1-15 s/min; 2–16-30 s/min; 3–31-45 s/min; 4–46-60 s/min] **(Supplementary Video 6, 7).**

Non-motor symptoms: Behaviors indicative of non-motor symptoms involving agitated locomotion were classified largely according to previous studies (Fox et al., 2010; Kwan et al., 2021; Visanji et al., 2009). Agitated rapid locomotion: Short episodes of very fast locomotion, typically running in circles. Ordinal scale from 0–4; Duration: [0 s/min – Absent; 1–1-15 s/min; 2–16-30 s/min; 3–31-45 s/min; 4–46-60 s/min], **(Supplementary Video 8).** Escape-like behavior: Rapidly approaching a corner of the behavioral box and forcefully jumping as if trying to escape. Ordinal scale from 0–4; Duration: [0 s/min – Absent; 1–1-15 s/min; 2–16-30 s/min; 3–31-45 s/min; 4–46-60 s/min], **(Supplementary Video 8).**

Hallucinations: At certain instances, the animals (mainly Monkey A) would show clear signs of visual hallucinations. Typically manifested as following non-apparent stimuli with their gaze for more than 10 s/min, and/or reaching and grasping for non-existing objects in thin air. These signs of visual hallucinations were scored in total amount of seconds, ordinal scale from 0–4; Duration: [0–10 s/min – Absent; 1–10-15 s/min; 2–16-30 s/min; 3–31-45 s/min; 4–46-60 s/min], **(Supplementary Video 9, 10).**

Signal acquisition

Local field potentials and unit activity (action potentials) were acquired using an OmniPlex D Neural Data Acquisition System (Plexon Inc.). The signal from the headstage pre-amplifier (6x gain, Nicolelis/Duke Headstage) was amplified between 4800 and 153000 times, high-pass filtered with cut-off 0.5 Hz, and digitized at 16 bits and 40 kHz. To obtain the local field potentials, the signal was low-pass filtered with a cut-off frequency of 300 Hz and down-sampled to 1000 Hz. Channels were visually inspected off-line for the presence of excessive noise and manually excluded from further analysis where appropriate. To obtain the spikes, the signal was high-pass filtered with a cut-off frequency of 600 Hz. Subsequently, 0.8-ms epochs around samples greater than 2.5 times the signal-noise were saved for off-line sorting.

Extraction of single unit activity

First, extracted spike events were temporally aligned and then clustered according to spike shape using a hierarchical clustering approach that enforced a 2-millisecond refractory period. Clusters with noise were identified by quantifying the spike density within the refractory window and clusters were excluded when this measure exceeded a value of 0.5%. The automated clustering produced 2,899 candidate clusters, of which 902 were retained after manual inspection. Units from different recording sessions were treated as independent, despite the possibility that the same neuron may have been recorded in more than one session.

Standardization of unit activity

Z-score was computed using the $(FR\text{-}\mu_{baseline})/ (\sigma_{baseline}+ \varepsilon)$, where $\mu_{baseline}$ and $\sigma_{baseline}$ are the mean and standard deviation of baseline firing rate, and ε is a small constant added to prevent division by zero.

Unit Analysis

The Wilcoxon rank-sum test was used to assess whether firing rates during the drug period differed from the corresponding baseline distribution. Units were classified as significantly down modulated if the median firing rate during the drug period was lower than the median baseline firing rate and the difference was statistically significant ($p < 0.05$). Conversely, units were classified as significantly up modulated if the median firing rate during the drug period exceeded the median baseline firing rate under the same significance criterion. Units that did not meet the significance criterion were classified as unchanged.

To compare the depth of modulation, we divided the drug periods into early and late periods. For classification of up and down modulated units, independent paired t-tests were used to evaluate differences in mean modulation between the two periods. In addition, a Wilcoxon signed-rank test was applied to assess differences from zero median modulation.

To determine whether the distribution of unit activity differed across brain structures, units were classified as up modulated, down modulated, or unchanged for each structure. A chi-square test of independence was used to assess whether the observed proportions significantly deviated from the

expected proportions across structures. Post hoc pairwise chi-square tests and Fisher's exact tests were subsequently performed to identify specific structural differences.

Finally, principal component analysis (PCA) was applied to firing rate data to characterize dominant temporal patterns of activity. The data was organized into a two-dimensional matrix where each row represents a single unit, and each column represents a time bin (40s). The temporal evolution of the first principal component was visualized, as it captures the dominant pattern of covariance across time.

Frequency analysis of local field potentials

Bipolar local field potential (LFP) time series were computed from all pairs of electrodes located in the same structure, to ensure that external sources contributed minimally to the local voltage fluctuations via volume conductance, thus emphasizing local sources.

Time-frequency power spectral densities (i.e. spectrograms) were calculated over the 0–250 Hz frequency range with 50% overlapping 8-s Hanning windows (0.12-Hz resolution) for each time series.

To emphasize oscillatory components in the power spectrum, we used irregular resampling (Wen & Liu, 2016). In brief, by resampling the time series multiple times, it is possible to separate the fractal (arrhythmic) component of the power spectrum. Subsequently, by normalizing the total spectrum to the fractal component, a power spectrum measure can be constructed that emphasizes truly rhythmic activity.

Peak Detection

To detect beta and narrowband gamma oscillations, we defined a parametric model,

$y(f) = A*exp\{-((f-B)/C)^2\} +Df + E$

which was fitted (Matlab fit function) to the spectra obtained by averaging together the spectra of individual electrode pairs from the same structure. The parameters A (peak height), B (peak frequency), C (peak width), D (inclination of flat background), and E (offset of flat background) were estimated such that the model y(f) fitted the spectrum optimally in the least-squares sense. This allowed us to detect beta/narrowband gamma peaks automatically by defining thresholds for the goodness-of-fit (R2) and the fitted parameters. Typical conditions for a positive detection were $R2 > 0.2$, $A > 2$ dB, with further parameter bounds set at $10 < B < 40$ Hz (beta) or $80 < B < 190$ Hz (narrowband gamma), $1 < C < 30$ Hz, $-1 < D < 1$, and $-10 < E < 10$. In the event of positive detections, the model was also used to quantify peak height, width and frequency parametrically.

Comparison between normalized spectra associated with dyskinesia and non-motor events

To reveal patterns in oscillatory activity associated with the presence of non-motor symptoms, we computed the normalized power spectral density over a restricted ± 1-minute window centered on each

detected non-motor symptom event. We then subtracted the normalized power spectral density computed over a 10-minute reference interval, selected near the peak dyskinesia time (approximately 1 hour after injection) and chosen to avoid any overlap with the non-motor symptom detection. The resulting differences emphasized changes in spectral content that were associated with non-motor symptom detections. We lowered the frequency resolution of these spectra by averaging within blocks of 5 Hz, producing 40 blocks (from [0,5] Hz until [195,200] Hz), and then plotted all individual events side-by-side, separately per structure and animal.

Additionally, we created a separate visualization for the subthalamic nucleus data only, where the spectra for all the non-motor symptom detection events (± 1 minute) were averaged, as well as the spectra for all the 10-minute reference intervals, but no subtraction was performed, and the full frequency resolution was kept. We then overlaid the two curves separately for each animal.

Tyrosine-hydroxylase staining and denervation quantification

The animals were sacrificed by intracardiac perfusion with 0.9% saline solution and heparin, followed by 4% paraformaldehyde. The brains were removed, dehydrated through sequential exposure to solutions of 20% and 30% sucrose and stored at − 80°C prior to 50 µm sectioning and staining. Immunohistochemical detection of tyrosine hydroxylase (TH) was performed with the rabbit primary anti-TH polyclonal, 1:500 (Merck, Germany) and the biotinylated goat anti-rabbit secondary antibody, 1:200 (Vector Labs, USA). The images were acquired with the ZEISS Axio Imager 2 microscope using either 5× or 20× objectives. TH-reactivity across the motor cortex, caudate, putamen, nucleus accumbens, internal globus pallidus and external globus pallidus was assessed by optical densitometry using ImageJ software (Santana et al., 2015). A contrast index for each brain area was then calculated (C = (G-W)/(G + W), where G is the average optical density of the region and W is the average optical density of the corpus callosum). TH-labeled cells in the ventral tegmental area/substantia nigra pars compacta (VTA/SNc) were counted in 4 sections of each animal with the StereoInvestigator system (MBF Bioscience Inc). The boundaries of the VTA/SNc were defined in each section, in the control side, according to an atlas (Paxinos et al., 2012).

Histological verification of recording sites

The positions of the recording electrodes were verified through cresyl violet staining of brain sections in both animals and only electrodes with tracks confirmed via histology were included in the further analyses (in total 7 channels in Monkey A and 61 Channels in Monkey B).

Results

Medial forebrain bundle 6-OHDA lesions induced extensive dopaminergic depletion in several cortico-basal ganglia

structures

For this study, we had access to two adult female common marmoset monkeys (Callithrix Jacchus). The two animals received neurotoxic lesions by 6-OHDA injections into the medial forebrain bundle, according to previously developed procedures (Annett et al., 1992; Santana et al., 2015). The extent of the lesions was quantified by immunohistochemistry for tyrosine hydroxylase (TH). There was a significant reduction in TH immunoreactivity in primary motor cortex (M1), caudate (Cd), putamen (Put), nucleus accumbens (Acb), external globus pallidus (GPe) and internal globus pallidus (GPi) in the lesioned compared to the intact hemisphere (Fig. 1A-C, $p < 0.05$). In Monkey A, the average intensity in the lesioned hemisphere was reduced to 63.5% ± 3.8% (M1), 44% ± 3.1% (Cd), 58.4 ± 2.0% (Put), 40.1% ± 1.2% (Acb), 52.1% ± 3.6% (GPe) and 39.9% ± 6.0% (GPi), while in Monkey B the average intensity was reduced to 30.3% ± 4.2% (M1), 15.4% ± 2.6% (Cd), 15.3% ± 2.3% (Put), 31.4% ± 2.1% (Acb), 23.9% ± 2.9% (GPe) and 17.4% ± 2.3% (GPi). Accordingly, there was also a significant reduction in the number of SN/VTA TH-positive cells in the lesioned compared to intact hemisphere in both Monkey A ($p = 0.010$, $U = 0$, **Fig. 1D**, left panel) and Monkey B ($p = 0.010$, $U = 0$, **Fig. 1D**, right panel). In relative terms, the number of dopaminergic neurons (number of cells/mm^2) in the lesioned midbrain was reduced to 30.73% ± 3.45% in Monkey A and to 37.56% ± 5.79% in Monkey B (it should be cautioned however, that tissue shrinkage following neurodegeneration complicated this latter cell density analysis). These results emphasize that although analyses of the extent of dopamine depletion in animal models of PD is commonly restricted to the Cd-Put (see e.g. Winkler et al., 2002), the loss of dopaminergic terminals can in fact be considerably more extensive and can independently affect several of the structures of the cortico-basal ganglia loop. This serves as a reminder that although pathophysiological conceptual models highlight the pronounced loss of dopamine in striatum, striatal denervation alone may not be sufficient to fully account for alterations in neuronal signaling in other parts of the basal ganglia arising as a consequence of the direct loss of dopaminergic tone in the different structures. But perhaps more importantly, because of the difference in lesion severity between the two animals (more severe in Monkey B), the response to chronic dopaminergic pharmacotherapy could here be assessed in primates representing somewhat different stages of PD.

Reversal of parkinsonism by dopaminergic replacement

To allow for detailed monitoring of behavioral changes in parallel with electrophysiological data collection, recordings were made in a relatively restricted environment (a transparent cubic box; 0.45 m side length) where the animals were free to spontaneously move around during the recording period (approximately 30 min baseline and up to 2h continued recording following drug injection). The L-DOPA doses used to alleviate PD-signs in unilaterally 6-OHDA lesioned non-human primates have in previous reports sometimes been considerably higher than typical clinical doses. In particular, a dose-response study using a quantitative rating scale of PD-signs indicated optimal doses in the range of 100–300 mg/kg (Kurlan et al., 1991). Hence, we here elected to use L-DOPA in different dose ranges in an interlaced design (one lower and one higher dose range: 30–75 and 150–200 mg/kg).

Unilateral 6-OHDA lesions in the common marmoset typically result in moderate hypokinesia (Santana et al., 2015). Nonetheless, quantitative assessments of changes in spontaneous motor behavior revealed that L-DOPA treatment significantly increased the amount of spontaneous locomotion, defined as the net translation of the body every second, already 15–30 min after L-DOPA injection, indicating reversal of hypokinesia (Fig. 2A, left; distance travelled on baseline compared with the drug onset period (1000-2000s after injection), Monkey A/B: $p < 0.002/p < 0.001$, paired t-test). This increase in spontaneous motor activity included an improved ability to initiate movement sequences, reflected in a significant increase in the frequency of initiated locomotion bouts ($p < 0.01/p < 0.001$, Fig. 2A, right). Signs of bradykinesia were also found to be reversed after L-DOPA treatment, as signified by a broad shift from slower to faster movement components in the distributions of movement speeds ($p < 0.001$, t-test, Fig. 2B; cf. Fuentes et al., 2009; Santana et al., 2014)

Finally, in Monkey B, neck dystonia/torticollis was observed during untreated conditions (Sambrook et al., 1979). This symptom was also significantly alleviated by L-DOPA (mean dystonia scores, at baseline vs. 30–60 min after L-DOPA treatment were: 1.88 OFF L-DOPA vs. 0.11 ON [$p < 0.001$, Wilcoxon rank sum], temporal plots for high and low dose L-DOPA are shown in Fig. 2C). Thus, on a behavioral level, a reduction of several characteristic signs of parkinsonism could be confirmed following L-DOPA treatment.

Behavioral changes observed following L-DOPA treatment were quantified using automated (panel A-B) and manual (C-E) assessment techniques. **A)** Reduction of hypokinesia, Left columns: Change in general motility, Right columns: Change in number of initiated locomotion bouts (behavior sampled prior to L-DOPA and 1000–2000 s after administration). **B)** Reduction of bradykinesia as indicated by a shift towards faster movement components (green = OFF and pink = ON L-DOPA). **C)** Time course of neck dystonia/torticollis in Monkey B. Effective symptomatic relief was observed after L-DOPA administration in both the lower (blue) and higher (orange) dose ranges. **D)** Temporal correlation matrix of abnormal behaviors (warm colors denote behaviors that tended to co-occur during the same 1-minute observation period and blue colors denote behaviors that tended to be mutually exclusive). **E)** Average frequency/severity scores of the five main categories of abnormal behaviors observed as a function of time after L-DOPA treatment, throughout the 2 h observation period.

Signs of excessive motor behavior induced by L-DOPA

While several archetypal parkinsonian motor signs were rapidly reversed (as expected), it was noted that L-DOPA treatment in many cases also induced a range of excessive motor behaviors that are not typically displayed by healthy animals. These abnormal behaviors were apparent shortly after the initial response to L-DOPA, starting approximately 30 minutes after injection and were displayed for prolonged periods during each recording session. Abnormal behaviors included both signs of dyskinesia (mainly manifested as dystonia in neck and limbs, and relatively less chorea) and hyperkinesia (indicated by excessive rotational behavior contraversive to the lesioned hemisphere), but also other abnormal behaviors suggestive of non-motor symptoms, such as signs of visual hallucinations (indicated by visual tracking of non-apparent stimuli and making reaching and grasping movements in the air; see

Supplementary videos 2–10 for examples of behaviors of each type). Other behaviors displayed were more ambiguous and have in previous studies been assigned to the psychiatric domain while being described in terms of their motor features (for example, episodes of rapid and agitated locomotion with no apparent goal, or escape-like jumping; Fox & Brotchie, 2010; Kwan et al., 2021). Hence, an overall increase in locomotion could possibly represent a combination of such non-motor signs and hyperkinesia belonging to the motor domain of symptoms.

We therefore divided these behaviors into five separate main symptom categories, ranging from most certainly motor (dystonia/dyskinesia) across ambiguous behaviors to most certainly non-motor (hallucinations). Assuming behavioral signs associated with a certain brain state occur in relative temporal proximity, we then analyzed to what extent behaviors in the different categories were present during the same 1-minute observation window, in each of the two monkeys. For this analysis we relied on manual scoring of videos collected during the neurophysiological recording sessions (for details see Methods). By correlating the observed behaviors in response to pharmacological treatment, over the time-course of each experiment, it became evident that signs of dystonia/dyskinesia and non-motor signs, practically never coincided during the same 1-minute observation window (P[motor|non-motor] < 0.07; and instead tended to be slightly anticorrelated; Fig. 2D). For ambiguous behaviors, such as excessive locomotion, a co-occurrence with both rotations and with non-motor behaviors was however observed. Thus, the temporal correlation analysis of the five main categories of excessive behaviors [Dystonia, Rotations, Excessive locomotion, Non-motor symptoms, Hallucinations] appeared to support the notion that while locomotion shows a certain overlap between non-motor/motor categories, these signs otherwise primarily reflect symptoms belonging either to the motor or non-motor domain.

Next, quantification of the five classes of L-DOPA-induced excessive behaviors was performed for both monkeys. Because the temporal profile of the behaviors differed (Fig. 2E), we analyzed each behavior up to 2h after L-DOPA injection. Comparing the average whole session scores to baseline, it was evident that all the observed behaviors were significantly increased in both animals ($p < 0.05$; paired Wilcoxon test), with the exception of the category of merged ‘non-motor symptoms’ in both animals and ‘hallucinations’ in Monkey B, which both had too few observations to reach significance (but which were never observed on baseline prior to L-DOPA injection). Hence, all signs in the motor domain were significantly increased whereas the non-motor signs showed a similar tendency, but only reached significance for hallucinations in Monkey A.

Since the two animals were tested over several months (detailed behavioral scoring was performed in Monkey A/B in 11/24 recordings over 237/365 days), and on two different dose ranges, it was possible to quantitatively compare behavioral signs separated at least 6 months in time at either high or low L-DOPA doses. Comparing behavioral scores from recording sessions obtained early (month 1–3) vs. late (month 6–12) and within the two different dose ranges, we observed a tendency for more dystonia at a higher dose (reaching significance in Monkey A, $p < 0.001$; 2-way ANOVA, Tukey post hoc test) but not in Monkey B (possibly due to a ceiling effect in this more severely lesioned animal). We also observed tendencies for a gradual decline in the amount of hyperkinesia (rotations) over time, comparing early vs.

late sessions (reaching significance in Monkey B, $p < 0.01$; 2-way ANOVA, Tukey post-hoc test). In this context it should be noted that certain behaviors are partially mutually exclusive, resulting in statistical interactions between symptom categories (for example, high levels of dystonia can be expected to mask other signs). Furthermore, dose responses may change over time causing an interaction between dose and time. Indeed, in Monkey B an interaction between time and dose was found for general locomotion ($p < 0.03$; 2-way ANOVA) – i.e. more locomotion was seen in early sessions on low dose. For the merged non-motor behaviors and hallucinations no significant differences depending on dose or time could be established. It should be noted, however, that the incidence of these behaviors was very low overall, and that hallucinations are particularly difficult to identify from video recordings with confidence, making it probable that such symptoms in fact were more common than what our present estimates suggest. In any case, while both time after lesion and L-DOPA dose to some extent affected the type of excessive motor behaviors displayed, there was no consistent pattern across the two animals, suggesting their individual patterns of dopaminergic denervation was a strongly contributing factor (cf. Figure 1).

L-DOPA pharmacotherapy induces acute circuit-wide changes in firing rates and long-term increases in STN modulation depth

According to classical pathophysiological models (Albin et al., 1989; DeLong, 1990), parkinsonism is associated with abnormal firing rates in parts of the cortico-basal ganglia circuits. Indeed, this notion partly originated from studies in primate models of PD, where, for example, abnormal tonic firing rates in the STN were found in the MPTP treated macaque (Miller & DeLong, 1987). Furthermore, comparing early to late stage PD patients, higher spontaneous STN firing rates have been reported in the late stage suggesting long-term changes in excitability that may be associated with disease progression and/or long-term L-DOPA treatment (Remple et al., 2011). Thus, to further clarify both how L-DOPA acutely modifies neuronal firing rates and to what extent long-term dopaminergic pharmacotherapy changes drug-induced responses, we conducted single unit recordings in conjunction with the above described behavioral assessments in the two monkeys. To allow for comparisons to human data, the analysis of single unit activity was primarily focused on the STN. However, to gain more systems-level perspective on the observed STN modulations, a few additional sensorimotor brain structures were also recorded (for an overview of electrode placement, see **Supplementary Table 1).** Since it is next to impossible to confidently identify the same single units across different recording sessions, we elected to treat units recorded in separate sessions as different neurons (this resulted in a total of 215 well isolated single neurons recorded in 29 channels over 42 recording sessions, on L-DOPA, in the two monkeys; **Supplementary Table 1)**.

First, to elucidate the dominating L-DOPA induced patterns of rate modulations, we performed a principal component analysis of the firing rate changes observed across all recorded units in the lesioned hemisphere of the two animals. Firing rates were averaged in 40-second time bins, during the first 50 minutes after L-DOPA injection (this comparatively short post-L-DOPA analysis window was chosen to reduce the risk that neurons were lost in the recordings during the investigated period). The analysis revealed that 81.9% of the variance explained (corresponding to the eigenvalue of the first principal

component; PC1) followed a distinct time course characterized by a gradual increase in modulation depth developing during the first 30 minutes, followed by a plateau-phase with relatively minor further changes (Fig. 3A, B**)**. That is, while the firing rates of individual cells could be either increased or decreased compared to baseline, corresponding to positive or negative PC1 loadings, a majority of cells nevertheless followed the same temporal pattern of relative rate changes, closely matching the expected time course for systemically administered L-DOPA to reach the brain and be converted to dopamine (Porras et al., 2014). This general temporal pattern, which broadly matched the onset of abnormal motor behaviors (cf. Figure 2E**)**, was found to be very similar also for the sub-group of all cells recorded in STN (with 79.2% of the variance explained in STN, Fig. 3B). Other than STN, three structures (primary somatosensory cortex [S1], the caudate-putamen [Cd-Put] and the medial geniculate nucleus of the thalamus [MGN]) were found to have sufficient number of neurons to allow for evaluation of firing rate changes induced by L-DOPA. Comparing the mean firing rates observed in the lesioned hemisphere during baseline (-15 to -5 minutes before L-DOPA), to another 10-minute observation window during the early ON period (30–40 minutes after L-DOPA) it was evident that all four structures contained relatively large fractions of cells that displayed significantly altered firing rates ($p < 0.05$; Wilcoxon sign rank) in response to L-DOPA treatment. In particular, a majority of upregulated cells was found, constituting nearly identical fractions in MGN, Cd-Put and STN, whereas S1 had a different relative distribution (Fig. 3C; $p < 0.05$, Chi square test, and pairwise post-tests). That is, somewhat unexpectedly, although the dopaminergic innervation density varies considerably between these deep structures (ranging from high in Cd-Put, intermediate in STN, to low in MGN), their rate modulations after L-DOPA were very similar. Notably, the observed increased firing rates in STN following antiparkinsonian pharmacotherapy may at first glance appear to contradict previous primate STN recordings (Miller & DeLong, 1987). However, earlier studies have not investigated single unit activity in primates with dyskinesia, making the current observations the first of their kind. Hence, the identified group of cells, showing increased firing rates in association with the onset of abnormal motor behaviors, may be contributing to dyskinetic symptoms. If so, the gradual worsening of side effects associated with long-term L-DOPA treatment experienced by many PD patients could potentially stem from an increasing contribution from this cell population. To test this hypothesis, we next investigated whether the changes in STN firing rates induced by L-DOPA treatment were of a similar magnitude during earlier recordings (performed month 1–3) compared to later recordings (month 4–12). Overall, the fractions of up/down-modulated cells were found to be largely unchanged (up/down: Early, 68%/16% vs. Late, 65%/13%, $P > 0.05$, chi square test). Similarly, the dominating temporal profiles of rate modulations were found to be very much alike (Pearson correlation between PC1 for STN early and late was $R^2 = 0.73$). In contrast, the depth of modulation was found to change significantly from early to late recordings. Specifically, the average firing rate increases of individual up-regulated STN neurons (comparing [-15 to -5 minutes] before L-DOPA to [30–40 minutes] after) were significantly higher in the late period (mean rate increases from OFF to ON: Early period, 24.8 Hz vs. Late, 31.6 Hz; $p < 0.0015$; Wilcoxon rank sum; Fig. 3D). Thus, while the exact role of the upregulated STN cells in relation to abnormal motor behavior remains to be determined, our results suggest that a sub-group of overactive cells could be contributing to progression of dyskinetic symptoms in conjunction with long-term L-DOPA treatment.

Single unit recordings in the lesioned hemisphere in the two monkeys revealed distinct firing rate changes following L-DOPA administration. **A)** Changes in normalized firing rates in all recorded neurons during the first 50 minutes after L-DOPA (firing rates were z-scored in relation to baseline and sorted according to their similarity to PC1 [see B]). **B)** Coefficients of PC1 for each 40-s time bin over the 50-minute recording period demonstrated that the most dominant changes in firing rates occurred gradually during the first 30 minutes. **C)** Fractions of cells showing significant changes in firing rates 30–40 minutes after L-DOPA compared to their baseline firing rates (-15 to -5 min prior to injection; number of neurons indicated next to each fraction). **D)** Top row: Normalized L-DOPA-induced changes in STN firing rates (values were z-scored to baseline). Left column: recordings obtained month 1–3 and Right column: month 4–12. Middle and bottom rows: Average changes in firing rates (mean and SEM) for significantly up-/down-regulated cells. Note that modulation depth became relatively more pronounced in the later recordings.

Beta-range LFP oscillations in cortico-basal ganglia circuits associated with the parkinsonian state are partly separable in frequency and are reduced by L-DOPA

With the advent of deep-brain stimulation (DBS) as an advanced therapy for PD, obtaining neuronal recordings in conjunction with implantation surgeries became possible. As a consequence, LFP dynamics has been relatively well characterized in the human STN, including changes related to L-DOPA treatment (see e.g. Alonso-Frech et al., 2006; Brown et al., 2001). In such recordings, beta range (13–35 Hz) oscillations have been a frequent observation in the OFF state. These synchronized oscillations are associated with bradykinetic symptoms and are reduced by both DBS and L-DOPA treatment (de Neeling et al., 2025; Hammond et al., 2007).

In line with the human data, enhanced beta activity has also been reported in the 6-OHDA marmoset model of PD (Santana et al., 2014). However, in this earlier study a state of more pronounced dopaminergic depletion was investigated, achieved by treating the 6-OHDA lesioned monkeys with the dopamine synthesis blocker alpha-methyl-p-tyrosine (AMPT). We therefore first examined if exaggerated beta oscillations could also be detected without additional pharmacological dopamine depletion. Unexpectedly, beta oscillations were reliably detected only in Monkey A, despite the fact that Monkey B had the more severe 6-OHDA lesion (possibly due to differences in electrode placements between the animals). In Monkey A, distinct beta oscillations were found both in STN and in pre-motor cortex (preM) in the lesioned hemisphere. As expected, this oscillatory activity was readily suppressed by L-DOPA treatment (parallel recordings from two pairs of electrodes located in preM and STN, respectively, in OFF and ON L-DOPA states are exemplified in Fig. 4A). It was evident that the amplitude of beta oscillations was higher in cortex than in STN in the 16 recordings ($p < 0.01$, paired t-test; but it needs to be cautioned that this difference could be partially explained by the varying cytoarchitecture of the two structures, since spatially aligned cells, as in cortex, can generate stronger combined electrical dipoles). Visual inspection of the LFPs in the temporal domain suggested several agreements with patterns observed in human studies. For example, beta activity tended to fluctuate in amplitude over periods of ∼1s, and showed a slightly non-sinusoidal wave-shape (Cole et al., 2017). With respect to frequency content, both

preM and STN appeared to display relatively increased LFP power in the lower beta-band, on top of a broader 1/f power distribution (Fig. 4B**).** Thus, to further emphasize the oscillatory component, all spectra were subsequently normalized to the non-periodic background of each recording. This analysis revealed great similarities between sessions recorded several months apart, both in the OFF and ON states (Fig. 4C). On average, the beta activity (around 13–18 Hz) was significantly reduced by L-DOPA in both structures (Fig. 4D; with mean reductions over the 16 recordings of 49.8% and 44.5%, for preM and STN, respectively, $p < 0.01$ and $p < 0.01$, paired t-test). It was also noted that in preM a relative power increase in parts of the higher beta band (> 20 Hz) could be observed (in accordance with earlier human studies suggesting that low-beta activity chiefly contributes to bradykinetic symptoms; Yin et al., 2021). In addition, a peak in the delta range (3–5 Hz) was detected OFF L-DOPA in STN. However, the functional role of these STN delta oscillations remains to be determined (oscillations in this frequency band [below tremor frequency (4–8 Hz)] have not commonly been found in awake parkinsonian primates). Examining beta suppression longitudinally across different sessions, no significant differences were observed between the low and high L-DOPA dose range or between early and late recording sessions (Fig. 4E; $p > 0.05$ N-way ANOVA). Finally, to investigate if the beta activity detected in preM and STN represented the same oscillations propagating through the cortico-basal ganglia system, we compared the peak frequency of 1050 individual 8-second periods with parallel detections of beta oscillations in the two structures. Interestingly, while we observed a general tendency for co-variation in peak frequency across oscillatory events, the STN peak frequency often did not reach as high as preM in the high-frequency episodes (Fig. 4F; $p < 0.001$, Pearson correlation). On average, preM had a peak frequency of 15.75 ± 1.75 Hz (mean ± SD) and peak width of 3.23 ± 1.90 Hz compared to 14.53 ± 2.46 Hz and 8.73 ± 4.00 Hz for STN. Thus, while oscillations in preM and STN are present simultaneously, the two structures do not strictly engage in shared oscillations of the same frequency.

L-DOPA-induced shifts in LFP low-frequency oscillatory components. **A)** Example raw traces from monopolar parallel LFP recordings in pre-motor cortex (preM) and STN, before (black) and after (red) L-DOPA treatment. **B)** Average LFP power spectra of preM and STN from 16 bipolar recording sessions OFF/ON L-DOPA (see panel E; 60 Hz spike is power-line noise). **C)** Individual bipolar power spectra from each recording after normalization to the power spectral density of the non-periodic component (dB Fractal). **D)** Average of the 16 spectra shown in panel C. **E)** Normalized peak power within the beta band across recording days 150–381 after lesioning. Green/purple fields mark session with the lower/higher L-DOPA dose range (gray/red bars mark OFF/ON L-DOPA). **F)** Comparisons of peak frequencies of concurrently recorded beta oscillations in preM and STN reveal minor frequency differences (equation inset represents linear fit to data [green dashed line] and the red line marks unity [1:1]). Mean and SD shown in panels B and D.

STN narrow-band gamma oscillations emerge following dopamine agonist treatment

In addition to the reversal of beta oscillations, a relative increase in LFP power in a narrow part of the gamma band (70–90 Hz) has often been observed in human STN recordings, which can become further

exaggerated in the presence of dyskinesia (Brown et al., 2001; Swann et al., 2016; see also, Alonso-Frech et al. 2006). However, even though clear behavioral changes were induced by L-DOPA in the two animals (cf. Figure 2), no evident LFP dynamics resembling human narrow-band gamma oscillations (NBGs) could be established. One hypothetical explanation for this discrepancy could be that the conversion efficiency of L-DOPA to dopamine in 6-OHDA lesioned marmosets is not fully comparable to human PD patients. This may result in differences in network dynamics and could also explain the much higher L-DOPA doses sometimes used (Kurlan et al., 1991). In this situation, direct activation of dopamine receptors via dopamine agonists could potentially induce electrophysiological changes more closely resembling the responses seen in humans at comparable doses. For this reason, L-DOPA was temporarily substituted with apomorphine in Monkey B (tested in a dose range of 0.3-2.0 mg/kg). Interestingly, in the very first apomorphine recording, evident NBGs emerged in STN (Fig. 5A, B). This finding was repeated in another eleven recording sessions on apomorphine performed in the subsequent weeks (it was also noted that on a behavioral level the antiparkinsonian effect of apomorphine resembled L-DOPA, and that neuronal firing rate changes followed a similar pattern to L-DOPA; see **Supplementary Fig. 1**). Surprisingly, however, when L-DOPA was reintroduced after this period of apomorphine treatment, NBGs were consistently found in STN also in the L-DOPA ON state (Fig. 5A). Yet, NBGs were not detected in any of the other structures recorded in parallel, for either apomorphine or L-DOPA (Fig. 5B, left and right column, respectively). It might be important to note that while the NBGs detected in Monkey B broadly resemble earlier human recordings, they appear to differ in two respects. First, human NBGs are primarily found in the 70–90 Hz range, whereas the NBGs in Monkey B had a higher peak frequency for both apomorphine and L-DOPA (peak frequency [mean ± SD]: 121.6 ± 9.6 Hz and peak width of 7.2 ± 2.8 Hz for apomorphine, and 124.4 ± 8.8 Hz and 7.8 ± 3.6 Hz for L-DOPA). Second, once the NBGs were established, similar oscillations were also observed in the OFF state in some recordings, **(**Fig. 5B, gray bars, albeit less pronounced than in the ON state), which is typically not the case in humans (Olaru et al., 2024).

Finally, because this study, to our knowledge, is the first encompassing neurophysiological recordings during discrete identified episodes of behavioral manifestations of PD-P, we reasoned it would be of interest to investigate if circuit dynamics in this state differs from the network dynamics associated with dyskinetic symptoms (although it needs to be acknowledged that this analysis had to be based on the small number of identified non-motor/hallucination events). To this aim, we first created an overview visualization of differences in network dynamics for all recorded structures, comparing episodes of identified PD-P manifestations to episodes with dyskinetic motor signs. Average power spectra were calculated +/- 1 minute around each PD-P event (where the symptom categories ‘non-motor symptoms’ and ’hallucinations’ in Monkey A and ‘hallucinations’ in Monkey B were included). These spectra were compared to those of a representative period (10 minutes) of prolonged dyskinesia from the same recording but separated from the corresponding PD-P event. Subtraction of all pairs of spectra suggested that STN was a structure of particular relevance for differentiation between the two states in both animals (Fig. 5C). Averaging the spectra over all events, our data suggest that the main state

differences [non-motor vs. motor] consist of relative shifts in the peak frequency of oscillatory components within the gamma band (40–140 Hz; Fig. 5D).

Drug-induced motor and non-motor signs were associated with changes in high-frequency oscillatory components. **A)** Temporal sequence of recordings showing that narrow-band gamma oscillations in the STN emerged in Monkey B after treatment with apomorphine and remained after switching back to L-DOPA treatment (gray bars mark baseline prior to drug injection, yellow apomorphine and red L-DOPA; shaded green and purple areas mark low and high L-DOPA dose ranges, respectively and shaded gray apomorphine). **B)** Spectrograms illustrating LFP oscillatory components in five structures recorded in parallel during the first apomorphine recording (left column) and the first subsequent L-DOPA recording (right column), demonstrating STN narrow-band gamma activity in both recordings. **C)** Overview of spectral differences between non-motor/hallucinations and dyskinesia-related brain activity across different structures in the two animals, based on 15 identified non-motor/hallucination events. Note the consistent differences in STN suggesting frequency shifts between the states in a limited part of the spectrum. **D)** Averaged STN normalized power spectral densities for non-motor/hallucinations vs. dyskinesia-related episodes suggest a main relative power difference in the gamma-band for the two animals (40–140 Hz and 110–140 Hz, respectively).

Discussion

In the present study, we analyzed behavioral and electrophysiological changes induced by dopamine replacement therapy, both acutely and over the long term, in two 6-OHDA lesioned marmosets. The behavioral responses to L-DOPA in the two monkeys were found to be largely comparable, in spite of differences in lesion severity indicated by the immunohistochemical quantification of TH-labeled terminal densities in cortico-basal ganglia structures, suggesting both lesions were sufficiently severe to induce robust parkinsonian signs and promote sensitization to dopamine. On the other hand, since the manifestations of levodopa-induced excessive behaviors were not entirely consistent between the two monkeys, when analyzed over the entire one-year treatment period, it is possible that differences in relative dopamine depletion may have contributed to interindividual differences in network plasticity over the long term. Excessive behaviors observed ranged from distinct motor signs such as dystonia to clear psychiatric signs, such as visual hallucinations. Although few earlier studies in 6-OHDA lesioned marmosets have characterized this broad spectrum of L-DOPA induced behaviors, some of the current observations closely resemble behaviors previously described in MPTP-treated marmosets indicative of motor and PD-P symptoms (Fox et al., 2009; Johnston et al., 2013; Kurlan et al., 1991; Kwan et al., 2021; Visanji et al., 2006).

In parallel with behavioral assessments, we recorded single unit activity and LFPs in distributed brain structures. For technical reasons the total number of units was rather limited and unevenly sampled across different brain structures. Yet, among the two animals, several parts of the cortico-basal ganglia-loop thought to contribute to hyperkinetic behavior were recorded (Cenci et al., 2018), as well as thalamic nuclei implicated in auditory and visual hallucinations (Mancini et al., 2020; Zhuo et al., 2020),

giving at least partial information about the wider network activity. Also, it should be emphasized that no previous longitudinal recordings exist of unit activity in primates characterizing neuronal L-DOPA responses both acutely and over extended time periods. Hence, the current data set represents an important first step towards a better understanding of the pathophysiology underlying side effects of PD medication. In this context, the present finding that a sub-group of neurons in STN displays significantly increased firing rates during periods of excessive L-DOPA-induced behaviors and, furthermore, shows gradually increasing modulation depth with long-term treatment, may provide important mechanistic information. Indeed, in line with our findings, a subpopulation of overactive STN neurons was recently described in the STN in a mouse model of LID. Although, optogenetically activating these neurons did not directly induce dyskinesia, making their causal relation to LID uncertain (Shen et al., 2024). In any case, the potential pathophysiological role of the much larger fraction of excited STN neurons observed in our L-DOPA treated parkinsonian primates clearly deserves further investigation.

It is known from several earlier studies that LFPs obtained from chronic recordings in dyskinetic PD-patients and from 6-OHDA lesioned rats, show almost identical NBGs with a peak around 70–90 Hz (Halje et al., 2012; Swann et al., 2016). In the current study, detected NBGs were restricted to the STN, and were observed only in the monkey with more severe dopaminergic denervation. Consequently, it can be speculated that the time needed for induction of network changes responsible for development of NBGs may be longer than one year for more moderate dopamine denervation, as in Monkey A. Importantly, it should be cautioned that it also remains unclear if the NBGs observed in Monkey B represent the same pathophysiological phenomenon as the previously described NBGs in rats and humans. In particular, based on rat studies, it has been suggested that while 70–90 Hz oscillations in sensorimotor circuits appear to be strongly associated with dyskinesia, high-frequency oscillations in cognitive-limbic structures in the higher gamma-band (110–160 Hz) could instead be related to psychosis-like states (Brys et al., 2023; Nasretdinov et al., 2023; Petersson et al., 2019). Hence, we here attempted to test for such a distinction in LFP activity patterns, by comparing recording periods with PD-P signs to other periods with dystonia/dyskinesia during the same recording session. Unfortunately, this analysis was limited by the small number of non-motor observations making it primarily descriptive. Nonetheless, the main difference observed in this comparison was indeed related to a shift in peak frequency within the gamma band, strengthening the notion of a link between the main oscillation frequency and the dominant type of symptoms experienced. It is important to keep in mind, however, that oscillatory frequency ranges may not be directly comparable between species. As an example, NBGs in dyskinetic mice have been reported to often occur in a higher frequency band than in rats and humans (with peak frequencies reaching up to 130 Hz), in this respect closer resembling the NBGs observed in Monkey B (Petersson & Walters, 2025).

In conclusion, this study represents the first characterization of neurophysiological features associated with long-term L-DOPA treatment in the extended cortico-basal ganglia circuits in parkinsonian primates. Our results point to overactivity of a fraction of STN neurons and NBGs in the higher gamma band as two pathophysiological phenomena potentially contributing to both motor and non-motor side effects, which we propose deserve further investigation.

Declarations

Author Contribution

M.A. Designed and performed experimentsG.I. Analyzed data and generated figuresL.Z. Analyzed data and generated figuresL.C. Analyzed data and generated figuresJ.R. Performed experimentsM.N. Performed experimentsP.H. Analyzed data and generated figuresR.F. Designed experimentsP.P. Designed experiments and wrote manuscriptAll authors reviewed the final version of the manuscript

Acknowledgement

The study was supported by grants from the Kempe Foundation, Insamlingsstiftelserna, Umeå University, The Swedish Parkinson Foundation, The Swedish Brain Foundation, Åhlén Foundation, Ebon Norlin Foundation, Konung Gustav Vs och Drottning Victorias foundation, Promobilia Foundation, MultiPark, and Vetenskapsrådet (VR) grant 2018–02717 and 2021 – 01769.

The computations were enabled by resources provided by the National Academic Infrastructure for Supercomputing in Sweden (NAISS), partially funded by the Swedish Research Council through grant agreement no. 2022–06725.

Data Availability

The data that support the findings of this study are available from the corresponding author upon reasonable request.

References

1. Albin, R. L., Young, A. B., & Penney, J. B. (1989). The functional anatomy of basal ganglia disorders. *Trends in Neurosciences*, *12*(10), 366–375. http://www.ncbi.nlm.nih.gov/pubmed/2479133
2. Alcacer, C., Andreoli, L., Sebastianutto, I., Jakobsson, J., Fieblinger, T., & MA, C. (2016). Chemogenetic stimulation of striatal projection neurons modulates responses to Parkinson's therapy. *Journal of Clinical Investigation*.
3. Alcacer, C., Klaus, A., Mendonça, M., Abalde, S. F., Cenci, M. A., & Costa, R. M. (2025). Abnormal hyperactivity of specific striatal ensembles encodes distinct dyskinetic behaviors revealed by high-resolution clustering. *Cell Reports*, *44*(7). https://doi.org/10.1016/j.celrep.2025.115988
4. Alonso-Frech, F., Zamarbide, I., Alegre, M., Rodríguez-Oroz, M. C., Guridi, J., Manrique, M., Valencia, M., Artieda, J., & Obeso, J. A. (2006). Slow oscillatory activity and levodopa-induced dyskinesias in Parkinson's disease. *Brain: A Journal of Neurology*, *129*(Pt 7), 1748–1757. https://doi.org/10.1093/brain/awl103

5. Annett, L. E., Rogers, D. C., Hernandez, T. D., & Dunnett, S. B. (1992). Behavioural analysis of unilateral monoamine depletion in the marmoset. *Brain: A Journal of Neurology*, *115 (Pt 3*, 825–856. http://www.ncbi.nlm.nih.gov/pubmed/1352726
6. Batzu, L., Podlewska, A., Gibson, L., Chaudhuri, K. R., & Aarsland, D. (2024). A general clinical overview of the non-motor symptoms in Parkinson's disease: Neuropsychiatric symptoms. *International Review of Neurobiology*, *174*, 59–97. https://doi.org/10.1016/BS.IRN.2023.11.001
7. Brown, P., Oliviero, A., Mazzone, P., Insola, A., Tonali, P., & Di Lazzaro, V. (2001). Dopamine Dependency of Oscillations between Subthalamic Nucleus and Pallidum in Parkinson's Disease. *Journal of Neuroscience*, *21*(3).
8. Brys, I., Barrientos, S. A., Ward, J. E., Wallander, J., Petersson, P., & Halje, P. (2023). 5-HT2AR and NMDAR psychedelics induce similar hyper-synchronous states in the rat cognitive-limbic cortex-basal ganglia system. *Communications Biology*, *6*(1). https://doi.org/10.1038/S42003-023-05093-6
9. Calon, F., Rajput, A. H., Hornykiewicz, O., Bédard, P. J., & Di Paolo, T. (2003). Levodopa-induced motor complications are associated with alterations of glutamate receptors in Parkinson's disease. *Neurobiology of Disease*, *14*(3), 404–416. https://doi.org/10.1016/J.NBD.2003.07.003
10. Carta, M., Carlsson, T., Kirik, D., & Björklund, A. (2007). Dopamine released from 5-HT terminals is the cause of L-DOPA-induced dyskinesia in parkinsonian rats. *Brain: A Journal of Neurology*, *130*(Pt 7), 1819–1833. https://doi.org/10.1093/brain/awm082
11. Cenci, A. M. (2007). Dopamine dysregulation of movement control in L-DOPA-induced dyskinesia. *Trends in Neurosciences*, *30*(5), 236–243. https://doi.org/10.1016/j.tins.2007.03.005
12. Cenci, M., Jörntell, H., & Petersson, P. (2018). On the neuronal circuitry mediating L-DOPA-induced dyskinesia. *Journal of Neural Transmission (Vienna, Austria: 1996)*. https://doi.org/10.1007/s00702-018-1886-0
13. Cole, S. R., van der Meij, R., Peterson, E. J., de Hemptinne, C., Starr, P. A., & Voytek, B. (2017). Nonsinusoidal Beta Oscillations Reflect Cortical Pathophysiology in Parkinson's Disease. *The Journal of Neuroscience*, *37*(18), 4830. https://doi.org/10.1523/JNEUROSCI.2208-16.2017
14. de Neeling, M. G. J., Keulen, B. J., Stam, M. J., Hubers, D., de Bie, R. M. A., van Wijk, B. C. M., Schuurman, P. R., Buijink, A. W. G., & Beudel, M. (2025). Beta Power Response After Levodopa Intake in Parkinson's Disease Patients With Chronic Sensing-Enabled Deep Brain Stimulation. *Annals of Neurology*. https://doi.org/10.1002/ANA.78025
15. DeLong, M. R. (1990). Primate models of movement disorders of basal ganglia origin. *Trends in Neurosciences*, *13*(7), 281–285. https://doi.org/10.1016/0166-2236(90)90110-V
16. Dettmer, A. M., & Suomi, S. J. (2014). Nonhuman Primate Models of Neuropsychiatric Disorders: Influences of Early Rearing, Genetics, and Epigenetics. *ILAR Journal*, *55*(2), 361–370. https://doi.org/10.1093/ILAR/ILU025
17. Dupre, K. B., Cruz, A. V, McCoy, A. J., Delaville, C., Gerber, C. M., Eyring, K. W., & Walters, J. R. (2015). Effects of L-dopa priming on cortical high beta and high gamma oscillatory activity in a rodent

model of Parkinson's disease. *Neurobiology of Disease*, *86*, 1–15. https://doi.org/10.1016/j.nbd.2015.11.009

18. Ek, F., Malo, M., M, Å. A., Wedding, C., Kronborg, J., Svensson, P., Waters, S., Petersson, P., & Olsson, R. (2016). *Behavioral analysis of dopaminergic activation in zebrafish and rats reveals similar phenotypes.* http://europepmc.org/abstract/med/26947759
19. Fénelon, G., & Alves, G. (2010). Epidemiology of psychosis in Parkinson's disease. *Journal of the Neurological Sciences*, *289*(1–2), 12–17. https://doi.org/10.1016/j.jns.2009.08.014
20. Forsaa, E. B., Larsen, J. P., Wentzel-Larsen, T., Goetz, C. G., Stebbins, G. T., Aarsland, D., & Alves, G. (2010). A 12-year population-based study of psychosis in Parkinson disease. *Archives of Neurology*, *67*(8), 996–1001. https://doi.org/10.1001/ARCHNEUROL.2010.166
21. Fox, S. H., & Brotchie, J. M. (2010). The MPTP-lesioned non-human primate models of Parkinson's disease. Past, present, and future. In *Progress in brain research* (Vol. 184, Number 10). Elsevier B.V. https://doi.org/10.1016/S0079-6123(10)84007-5
22. Fox, S. H., Visanji, N., Reyes, G., Huot, P., Gomez-ramirez, J., Johnston, T., & Brotchie, J. M. (2009). *Neuropsychiatric Behaviors in the MPTP Marmoset Model of Parkinson ' s Disease*.
23. Fox, S. H., Visanji, N., Reyes, G., Huot, P., Gomez-Ramirez, J., Johnston, T., & Brotchie, J. M. (2010). Neuropsychiatric behaviors in the MPTP marmoset model of Parkinson's disease. *The Canadian Journal of Neurological Sciences. Le Journal Canadien Des Sciences Neurologiques*, *37*(1), 86–95. http://www.ncbi.nlm.nih.gov/pubmed/20169779
24. Fuentes, R., Petersson, P., Siesser, W. B., Caron, M. G., & Nicolelis, M. A. L. (2009). Spinal cord stimulation restores locomotion in animal models of Parkinson's disease. *Science (New York, N.Y.)*, *323*(5921), 1578–1582. https://doi.org/10.1126/science.1164901
25. Güttler, C., Altschüler, J., Tanev, K., Böckmann, S., Haumesser, J. K., Nikulin, V. V., Kühn, A. A., & van Riesen, C. (2021). Levodopa-Induced Dyskinesia Are Mediated by Cortical Gamma Oscillations in Experimental Parkinsonism. *Movement Disorders: Official Journal of the Movement Disorder Society*, *36*(4), 927–937. https://doi.org/10.1002/MDS.28403
26. Halje, P., Tamtè, M., Richter, U., Mohammed, M., Cenci, M. A., & Petersson, P. (2012). Levodopa-induced dyskinesia is strongly associated with resonant cortical oscillations. *The Journal of Neuroscience: The Official Journal of the Society for Neuroscience*, *32*(47), 16541–16551. https://doi.org/10.1523/JNEUROSCI.3047-12.2012
27. Hammond, C., Bergman, H., & Brown, P. (2007). Pathological synchronization in Parkinson's disease: networks, models and treatments. *Trends in Neurosciences*, *30*(7), 357–364. https://doi.org/10.1016/j.tins.2007.05.004
28. Johnston, T. H., Huot, P., Damude, S., Fox, S. H., Jones, S. W., Rusche, J. R., & Brotchie, J. M. (2013). RGFP109, a histone deacetylase inhibitor attenuates l-DOPA-induced dyskinesia in the MPTP-lesioned marmoset: A proof-of-concept study. *Parkinsonism and Related Disorders*, *19*(2), 260–264. https://doi.org/10.1016/j.parkreldis.2012.07.001

29. Kurlan, R., Kim, M. H., & Gash, D. M. (1991). Oral levodopa dose-response study in MPTP-induced hemiparkinsonian monkeys: assessment with a new rating scale for monkey parkinsonism. *Movement Disorders: Official Journal of the Movement Disorder Society*, *6*(2), 111–118. https://doi.org/10.1002/MDS.870060205
30. Kwan, C., Nuara, S. G., Gourdon, J. C., & Huot, P. (2021). Further characterisation of psychosis-like behaviours induced by L-DOPA in the MPTP-lesioned marmoset. *Naunyn-Schmiedeberg's Archives of Pharmacology*, *394*(8), 1685–1692. https://doi.org/10.1007/S00210-021-02090-6
31. Mancini, V., Zöller, D., Schneider, M., Schaer, M., & Eliez, S. (2020). Abnormal Development and Dysconnectivity of Distinct Thalamic Nuclei in Patients With 22q11.2 Deletion Syndrome Experiencing Auditory Hallucinations. *Biological Psychiatry: Cognitive Neuroscience and Neuroimaging*, *5*(9), 875–890. https://doi.org/10.1016/J.BPSC.2020.04.015
32. Miller, W. C., & DeLong, M. R. (1987). *Altered Tonic Activity of Neurons in the Globus Pallidus and Subthalamic Nucleus in the Primate MPTP Model of Parkinsonism*. 415–427. https://doi.org/10.1007/978-1-4684-5347-8_29
33. Nasretdinov, A., Barrientos, S. A., Brys, I., Halje, P., & Petersson, P. (2023). Systems-level analysis of local field potentials reveals differential effects of lysergic acid diethylamide and ketamine on neuronal activity and functional connectivity. *Frontiers in Neuroscience*, *17*. https://doi.org/10.3389/FNINS.2023.1175575
34. Nelson, E. E., & Winslow, J. T. (2008). Non-Human Primates: Model Animals for Developmental Psychopathology. *Neuropsychopharmacology 2009 34:1*, *34*(1), 90–105. https://doi.org/10.1038/npp.2008.150
35. Olaru, M., Cernera, S., Hahn, A., Wozny, T. A., Anso, J., De Hemptinne, C., Little, S., Neumann, W. J., Abbasi-Asl, R., & Starr, P. A. (2024). Motor network gamma oscillations in chronic home recordings predict dyskinesia in Parkinson's disease. *Brain*, *147*(6), 2038–2052. https://doi.org/10.1093/BRAIN/AWAE004
36. Palmér, T., Ek, F., Enqvist, O., Olsson, R., Åström, K., & Petersson, P. (2017). Action sequencing in the spontaneous swimming behavior of zebrafish larvae - implications for drug development. *Scientific Reports*. https://doi.org/10.1038/s41598-017-03144-7
37. Paxinos, H., Watson, C., Petrides, M., osa, M., & Tokuno, H. (2012). *The Marmoset Brain in Stereotaxic Coordinates*.
38. Petersson, P., Halje, P., & Cenci, A. M. (2019). Significance and Translational Value of High-Frequency Cortico-Basal Ganglia Oscillations in Parkinson's Disease. *Journal of Parkinson's Disease*, *9*(1), 183–196. https://doi.org/10.3233/JPD-181480
39. Petersson, P., Kühn, A. A., Neumann, W. J., & Fuentes, R. (2020). Basal ganglia oscillations as biomarkers for targeting circuit dysfunction in Parkinson's disease. In *Progress in Brain Research* (Vol. 252, pp. 525–557). Elsevier B.V. https://doi.org/10.1016/bs.pbr.2020.02.002
40. Petersson, P., & Walters, J. R. (2025). Network dynamics in rodent models of Parkinson's disease. *Handbook of Behavioral Neuroscience*, *35*, 321–341. https://doi.org/10.1016/B978-0-443-21992-

4.00016-6

41. Porras, G., De Deurwaerdere, P., Li, Q., Marti, M., Morgenstern, R., Sohr, R., Bezard, E., Morari, M., & Meissner, W. G. (2014). L-dopa-induced dyskinesia: Beyond an excessive dopamine tone in the striatum. *Scientific Reports*, *4*(1), 1–5. https://doi.org/10.1038/SREP03730;SUBJMETA
42. Remple, M. S., Bradenham, C. H., Kao, C. C., Charles, P. D., Neimat, J. S., & Konrad, P. E. (2011). Subthalamic Nucleus Neuronal Firing Rate Increases with Parkinson's Disease Progression. *Movement Disorders: Official Journal of the Movement Disorder Society*, *26*(9), 1657. https://doi.org/10.1002/MDS.23708
43. Ryan, M. B., Bair-Marshall, C., & Nelson, A. B. (2018). Aberrant Striatal Activity in Parkinsonism and Levodopa-Induced Dyskinesia. *Cell Reports*, *23*(12), 3438–3446.e5. https://doi.org/10.1016/j.celrep.2018.05.059
44. Ryan, M. B., Girasole, A. E., Flores, A. J., Twedell, E. L., McGregor, M. M., Brakaj, R., Paletzki, R. F., Hnasko, T. S., Gerfen, C. R., & Nelson, A. B. (2024). Excessive firing of dyskinesia-associated striatal direct pathway neurons is gated by dopamine and excitatory synaptic input. *Cell Reports*, *43*(8). https://doi.org/10.1016/J.CELREP.2024.114483
45. Sambrook, M. A., Crossman, A. R., & Slater, P. (1979). Experimental torticollis in the marmoset produced by injection of 6-hydroxydopamine into the ascending nigrostriatal pathway. *Experimental Neurology*, *63*(3), 583–593. https://doi.org/10.1016/0014-4886(79)90173-0
46. Santana, M., Halje, P., Simplício, H., Richter, U., Freire, M. A., Petersson, P., Fuentes, R., & Nicolelis, M. (2014). *Spinal cord stimulation alleviates motor deficits in a primate model of Parkinson disease*. https://doi.org/10.1016/j.neuron.2014.08.061
47. Santana, M., Palmér, T., Simplício, H., Fuentes, R., & Petersson, P. (2015). Characterization of long-term motor deficits in the 6-OHDA model of Parkinson's disease in the common marmoset. *Behavioural Brain Research*. https://doi.org/10.1016/j.bbr.2015.04.037
48. Sellnow, R. C., Newman, J. H., Chambers, N., West, A. R., Steece-Collier, K., Sandoval, I. M., Benskey, M. J., Bishop, C., & Manfredsson, F. P. (2019). Regulation of dopamine neurotransmission from serotonergic neurons by ectopic expression of the dopamine D2 autoreceptor blocks levodopa-induced dyskinesia. *Acta Neuropathologica Communications*, *7*(1), 8. https://doi.org/10.1186/s40478-018-0653-7
49. Shen, C., Shen, B., Liu, D., Han, L., Zou, K., Gan, L., Ren, J., Wu, B., Tang, Y., Zhao, J., Sun, Y., Liu, F., Yu, W., Yao, H., Wu, J., & Wang, J. (2024). Bidirectional regulation of levodopa-induced dyskinesia by a specific neural ensemble in globus pallidus external segment. *Cell Reports. Medicine*, *5*(6). https://doi.org/10.1016/J.XCRM.2024.101566
50. Skovgård, K., Barrientos, S. A., Petersson, P., Halje, P., & Cenci, M. A. (2023). Distinctive Effects of D1 and D2 Receptor Agonists on Cortico-Basal Ganglia Oscillations in a Rodent Model of L-DOPA-Induced Dyskinesia. *Neurotherapeutics*, *20*(1), 304–324. https://doi.org/10.1007/s13311-022-01309-5

51. Stephan, H., Schwerdtfeger, W. K., & Baron, G. (1980). The Brain of the Common Marmoset (Callithrix jacchus). *The Brain of the Common Marmoset (Callithrix Jacchus)*. https://doi.org/10.1007/978-3-642-67491-4

52. Swann, N. C., de Hemptinne, C., Miocinovic, S., Qasim, S., Wang, S. S., Ziman, N., Ostrem, J. L., San Luciano, M., Galifianakis, N. B., & Starr, P. A. (2016). Gamma Oscillations in the Hyperkinetic State Detected with Chronic Human Brain Recordings in Parkinson's Disease. *The Journal of Neuroscience: The Official Journal of the Society for Neuroscience*, *36*(24), 6445–6458. https://doi.org/10.1523/JNEUROSCI.1128-16.2016

53. Tamtè, M., Brys, I., Richter, U., Ivica, N., Halje, P., & Petersson, P. (2016). Systems-level neurophysiological state characteristics for drug evaluation in an animal model of levodopa-induced dyskinesia. *Journal of Neurophysiology*, *115*(3), 1713–1729. https://doi.org/10.1152/jn.00868.2015

54. Visanji, N. P., Fox, S. H., Johnston, T., Reyes, G., Millan, M. J., & Brotchie, J. M. (2009). Dopamine D3 receptor stimulation underlies the development of L-DOPA-induced dyskinesia in animal models of Parkinson's disease. *Neurobiology of Disease*, *35*(2), 184–192. https://doi.org/10.1016/J.NBD.2008.11.010

55. Visanji, N. P., Gomez-Ramirez, J., Johnston, T. H., Pires, D., Voon, V., Brotchie, J. M., & Fox, S. H. (2006). Pharmacological characterization of psychosis-like behavior in the MPTP-lesioned nonhuman primate model of Parkinson's disease. *Movement Disorders: Official Journal of the Movement Disorder Society*, *21*(11), 1879–1891. https://doi.org/10.1002/mds.21073

56. Weintraub, D. (2020). Management of psychiatric disorders in Parkinson's disease: Neurotherapeutics - Movement Disorders Therapeutics. *Neurotherapeutics*, *17*(4), 1511. https://doi.org/10.1007/S13311-020-00875-W

57. Wen, H., & Liu, Z. (2016). Separating Fractal and Oscillatory Components in the Power Spectrum of Neurophysiological Signal. *Brain Topography*, *29*(1), 13–26. https://doi.org/10.1007/s10548-015-0448-0

58. Winkler, C., Kirik, D., Björklund, A., & Cenci, M. A. (2002). L-DOPA-induced dyskinesia in the intrastriatal 6-hydroxydopamine model of parkinson's disease: relation to motor and cellular parameters of nigrostriatal function. *Neurobiology of Disease*, *10*(2), 165–186. http://www.ncbi.nlm.nih.gov/pubmed/12127155

59. Yin, Z., Zhu, G., Zhao, B., Bai, Y., Jiang, Y., Neumann, W. J., Kühn, A. A., & Zhang, J. (2021). Local field potentials in Parkinson's disease: A frequency-based review. *Neurobiology of Disease*, *155*. https://doi.org/10.1016/j.nbd.2021.105372

60. Zahodne, L. B., & Fernandez, H. H. (2010). Parkinson's Psychosis. *Current Treatment Options in Neurology*, *12*(3), 200. https://doi.org/10.1007/S11940-010-0072-Y

61. Zhuo, C., Tian, H., Fang, T., Li, R., Li, Y., Kong, L., Cai, Z., Zheng, L., Lin, X., & Chen, C. (2020). Neural mechanisms underlying visual and auditory processing impairments in schizophrenia: insight into the etiology and implications for tailoring preventive and therapeutic interventions. *American Journal of Translational Research*, *12*(12), 7657–7669. https://pubmed.ncbi.nlm.nih.gov/33437351/

Figures

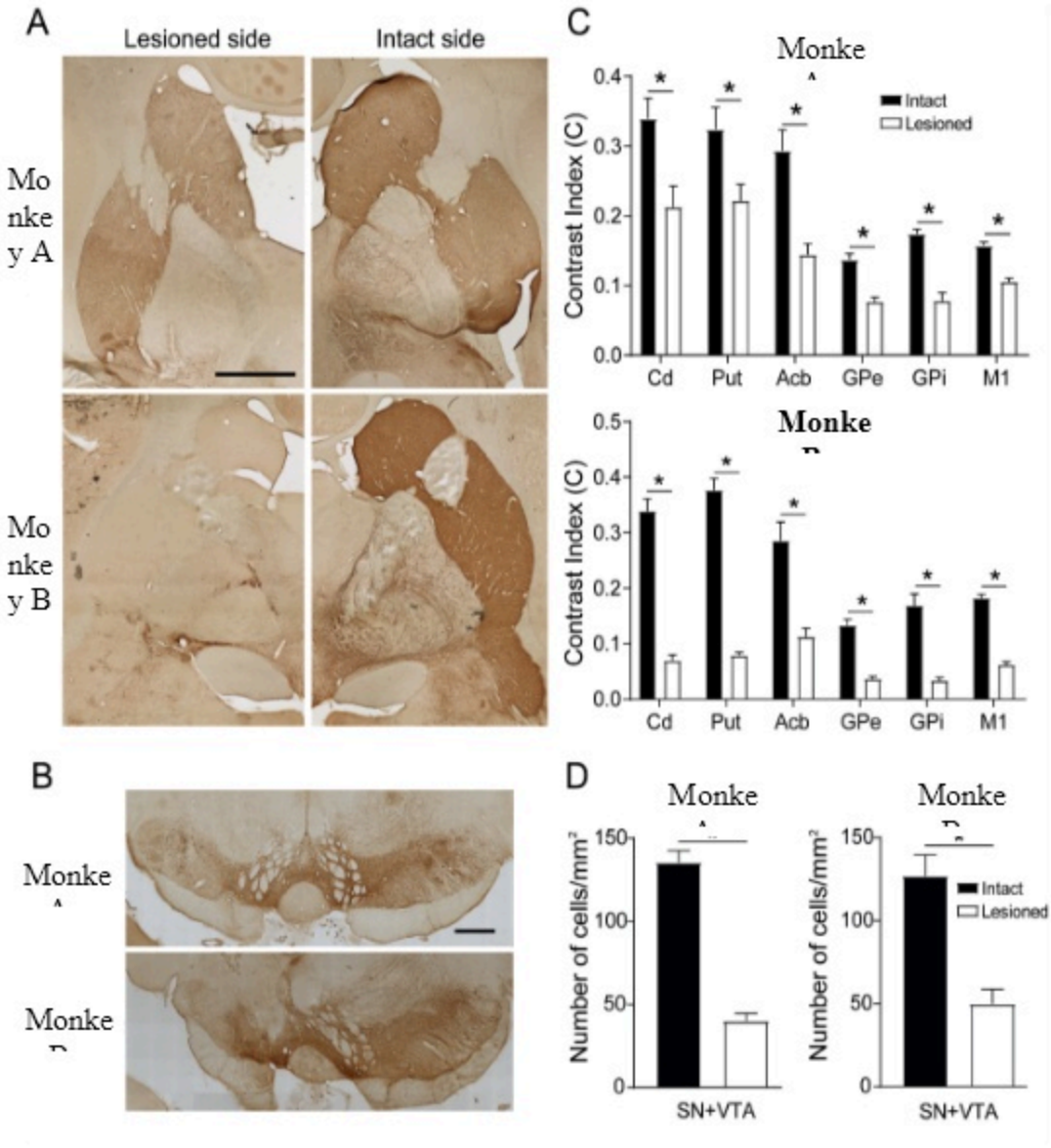

Figure 1

6-OHDA administration causes loss of dopaminergic innervation in cortico-basal ganglia structures. Two marmosets (Monkey A and B) were injected with 6-OHDA in the left medial forebrain bundle. The extent of dopaminergic denervation was assessed by TH-immunolabeling. **A**) Representative images of the TH immunostaining in the caudate (Cd), putamen (Put), globus pallidus externus (GPe) and globus pallidus internus (GPi; scale bar = 2000 µm). **B**) Representative images of TH immunostaining in substantia nigra (SN) and ventral tegmental area (VTA; scale bar = 1000 µm). **C**) Quantitative summary of TH staining in the Cd, Put, GPe, GPi, nucleus accumbens (Acb) andprimary motor cortex (M1), expressed as contrast index. **D**) Quantitative summary of cell body counts in the SN+VTA. Bar graphs show median ± SEM; *, $p < 0.05$, Mann-Whitney test.

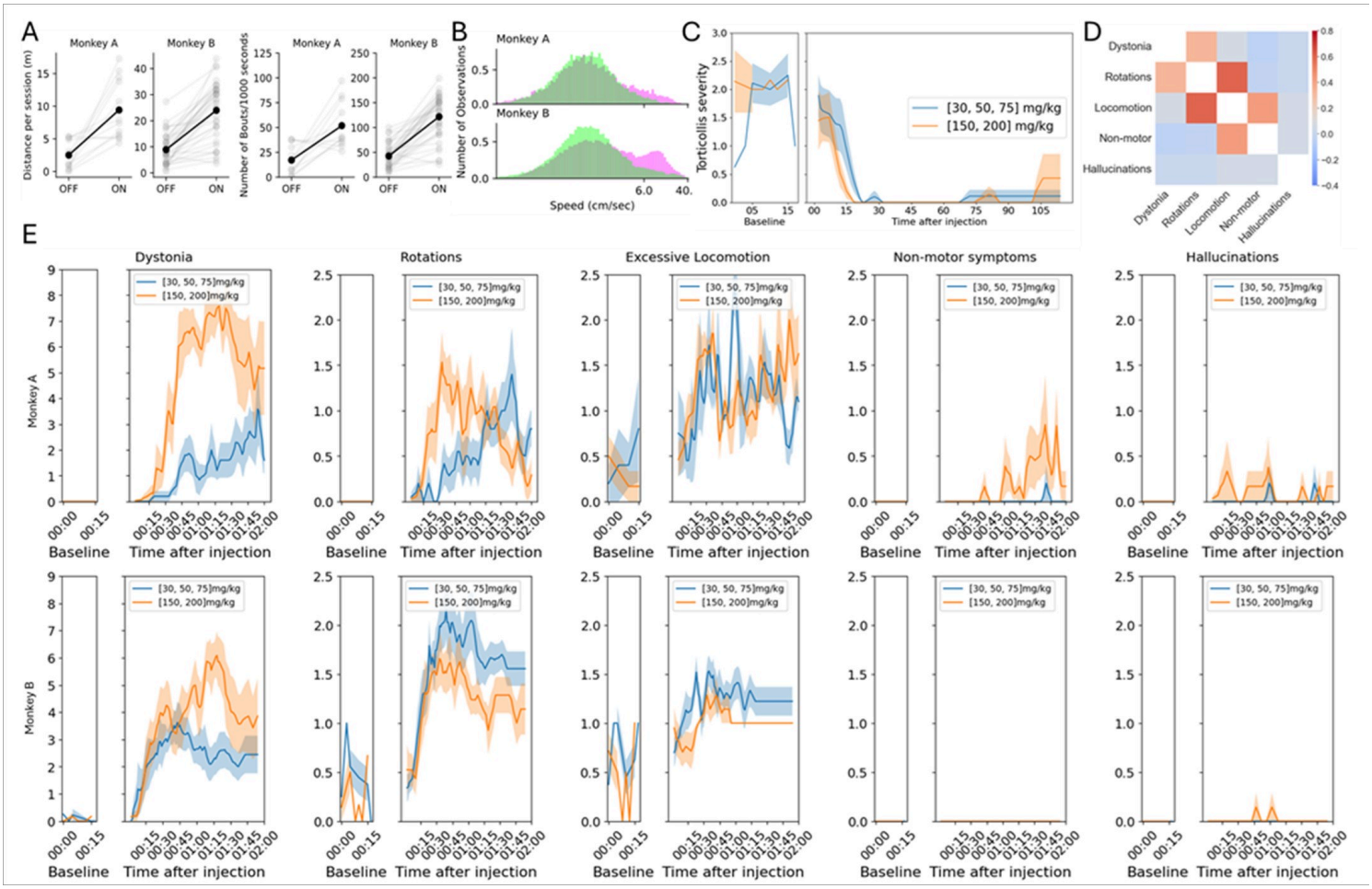

Figure 2

L-DOPA treatment reverses parkinsonism and induces excessive motor behaviors

Behavioral changes observed following L-DOPA treatment were quantified using automated (panel A-B) and manual (C-E) assessment techniques. **A)** Reduction of hypokinesia, Left columns: Change in general motility, Right columns: Change in number of initiated locomotion bouts (behavior sampled prior to L-DOPA and 1000-2000 s after administration). **B)**Reduction of bradykinesia as indicated by a shift towards faster movement components (green = OFF and pink = ON L-DOPA). **C)** Time course of neck dystonia/torticollis in Monkey B. Effective symptomatic relief was observed after L-DOPA administration in both the lower (blue) and higher (orange) dose ranges. **D)**Temporal correlation matrix of abnormal behaviors (warm colors denote behaviors that tended to co-occur during the same 1-minute observation period and blue colors denote behaviors that tended to be mutually exclusive). **E)** Average frequency/severity scores of the five main categories of abnormal behaviors observed as a function of time after L-DOPA treatment, throughout the 2 h observation period.

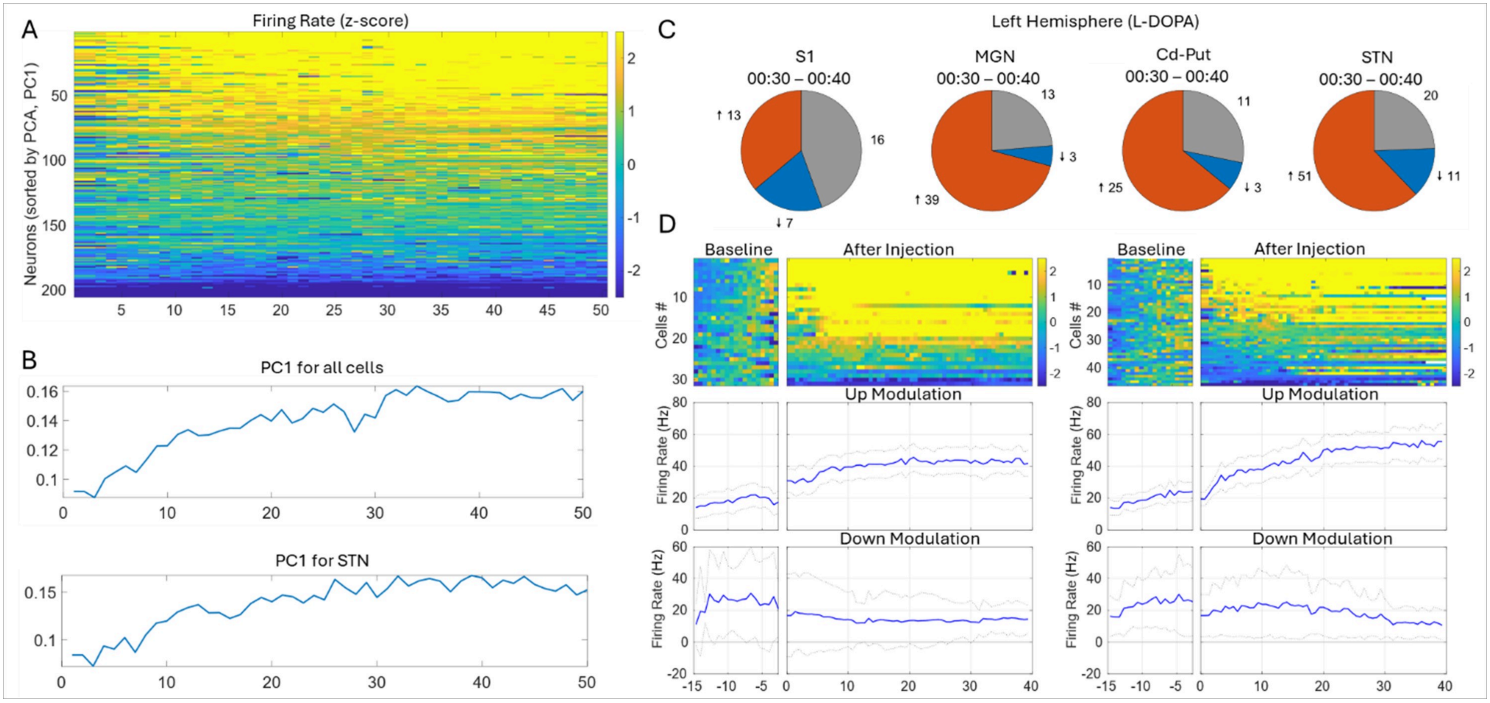

Figure 3

Changes in neuronal firing patterns induced by L-DOPA treatment

Single unit recordings in the lesioned hemisphere in the two monkeys revealed distinct firing rate changes following L-DOPA administration. **A)** Changes in normalized firing rates in all recorded neurons during the first 50 minutes after L-DOPA (firing rates were z-scored in relation to baseline and sorted according to their similarity to PC1 [see B]). **B)** Coefficients of PC1 for each 40-s time bin over the 50-minute recording period demonstrated that the most dominant changes in firing rates occurred gradually during the first 30 minutes. **C)**Fractions of cells showing significant changes in firing rates 30-40 minutes after L-DOPA compared to their baseline firing rates (-15 to -5 min prior to injection; number of neurons indicated next to each fraction). **D)** Top row: Normalized L-DOPA-induced changes in STN firing rates (values were z-scored to baseline). Left column: recordings obtained month 1-3 and Right column: month 4-12. Middle and bottom rows: Average changes in firing rates (mean and SEM) for significantly up-/down-regulated cells. Note that modulation depth became relatively more pronounced in the later recordings.

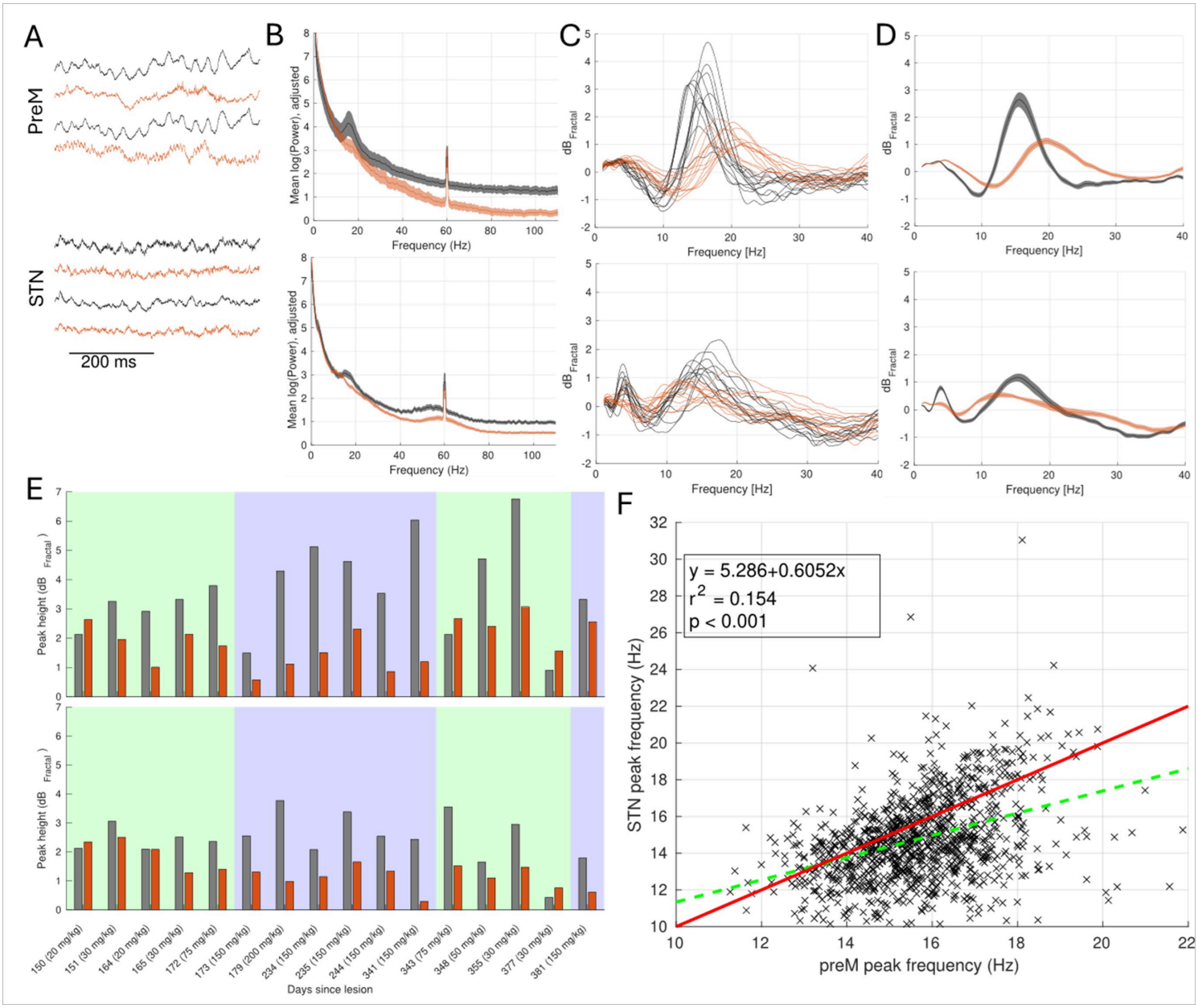

Figure 4

Beta oscillations in cortex and STN covary but are separable

L-DOPA-induced shifts in LFP low-frequency oscillatory components. **A)** Example raw traces from monopolar parallel LFP recordings in pre-motor cortex (preM) and STN, before (black) and after (red) L-DOPA treatment. **B)**Average LFP power spectra of preM and STN from 16 bipolar recording sessions OFF/ON L-DOPA (see panel E; 60 Hz spike is power-line noise). **C)** Individual bipolar power spectra from each recording after normalization to the power spectral density of the non-periodic component (dB Fractal). **D)** Average of the 16 spectra shown in panel C. **E)**Normalized peak power within the beta band across recording days 150-381 after lesioning. Green/purple fields mark session with the lower/higher L-DOPA dose range (gray/red bars mark OFF/ON L-DOPA). **F)**Comparisons of peak frequencies of concurrently recorded beta oscillations in preM and STN reveal minor frequency differences (equation

inset represents linear fit to data [green dashed line] and the red line marks unity [1:1]). Mean and SD shown in panels B and D.

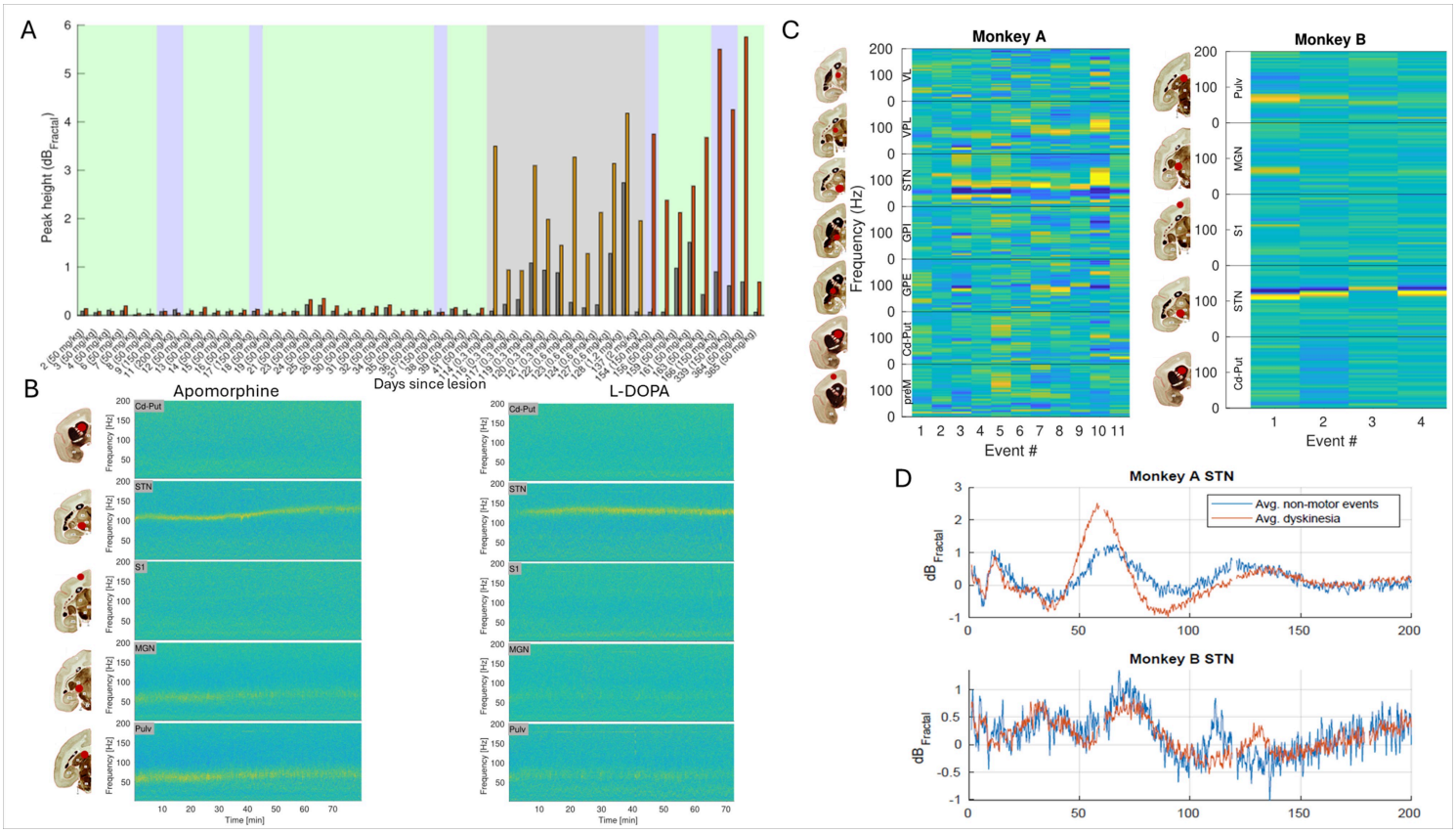

Figure 5

LFP spectral components associated with excessive motor behavior

Drug-induced motor and non-motor signs were associated with changes in high-frequency oscillatory components. **A)**Temporal sequence of recordings showing that narrow-band gamma oscillations in the STN emerged in Monkey B after treatment with apomorphine and remained after switching back to L-DOPA treatment (gray bars mark baseline prior to drug injection, yellow apomorphine and red L-DOPA; shaded green and purple areas mark low and high L-DOPA dose ranges, respectively and shaded gray apomorphine). **B)**Spectrograms illustrating LFP oscillatory components in five structures recorded in parallel during the first apomorphine recording (left column) and the first subsequent L-DOPA recording (right column), demonstrating STN narrow-band gamma activity in both recordings. **C)** Overview of spectral differences between non-motor/hallucinations and dyskinesia-related brain activity across different structures in the two animals, based on 15 identified non-motor/hallucination events. Note the consistent differences in STN suggesting frequency shifts between the states in a limited part of the spectrum. **D)**Averaged STN normalized power spectral densities for non-motor/hallucinations vs. dyskinesia-related episodes suggest a main relative power difference in the gamma-band for the two animals (40-140 Hz and 110-140 Hz, respectively).

Supplementary Files

This is a list of supplementary files associated with this preprint. Click to download.

- SupplementaryVideo1MonkeyBTorticollis.mp4
- SupplementaryVideo2MonkeyADyskinesia.mp4
- SupplementaryVideo3MokeyBDyskinesia.mp4
- SupplementaryVideo4MonkeyARotations.mp4
- SupplementaryVideo5MonkeyBRotations.mp4
- SupplementaryVideo6MonkeyAExcessiveLocomotion.mp4
- SupplementaryVideo7MonkeyBExcessiveLocomotion.mp4
- SupplementaryVideo8MonkeyAEscapeLikeBehaviorandAgitatedRapidLocomotion.mp4
- SupplementaryVideo9MonkeyBHallucination.mp4
- SupplementaryVideo10MonkeyAHallucination.mp4
- TablefigS1.docx